APL Materials

Electronic reconstruction at the polar (111)-oriented oxide interface

Cite as: APL Mater. **10**, 031115 (2022); https://doi.org/10.1063/5.0067445
Submitted: 16 August 2021 • Accepted: 17 February 2022 • Published Online: 29 March 2022

S. Ryu, H. Zhou, T. R. Paudel, et al.

Electronic reconstruction at the polar (111)-oriented oxide interface

Cite as: APL Mater. 10, 031115 (2022); doi: 10.1063/5.0067445
Submitted: 16 August 2021 • Accepted: 17 February 2022 •
Published Online: 29 March 2022

View Online Export Citation CrossMark

S. Ryu,[1] H. Zhou,[2] T. R. Paudel,[3] N. Campbell,[4] J. Podkaminer,[1] C. W. Bark,[1] T. Hernandez,[4] D. D. Fong,[5] Y. Zhang,[6] L. Xie,[6] X. Q. Pan,[6,7] E. Y. Tsymbal,[4] M. S. Rzchowski,[3] and C. B. Eom[1,a)]

AFFILIATIONS

[1] Department of Materials Science and Engineering, University of Wisconsin, Madison, Wisconsin 53706, USA
[2] X-ray Science Division, Argonne National Laboratory, Argonne, Illinois 60439, USA
[3] Department of Physics and Astronomy, University of Nebraska, Lincoln, Nebraska 68588, USA
[4] Department of Physics, University of Wisconsin, Madison, Wisconsin 53706, USA
[5] Materials Science Division, Argonne National Laboratory, Argonne, Illinois 60439, USA
[6] Department of Materials Science and Engineering, University of Michigan, Ann Arbor, Michigan 48109, USA
[7] Department of Materials Science and Engineering, University of California, Irvine, California 92697, USA

[a)] **Author to whom correspondence should be addressed:** eom@engr.wisc.edu

ABSTRACT

Atomically flat (111) interfaces between insulating perovskite oxides provide a landscape for new electronic phenomena. For example, the graphene-like coordination between interfacial metallic ion layer pairs can lead to topologically protected states [Xiao *et al.*, Nat. Commun. **2**, 596 (2011) and A. Rüegg and G. A. Fiete, Phys. Rev. B **84**, 201103 (2011)]. The metallic ion/metal oxide bilayers that comprise the unit cell of the perovskite (111) heterostructures require the interface to be polar, generating an intrinsic polar discontinuity [Chakhalian *et al.*, Nat. Mater. **11**, 92 (2012)]. Here, we investigate epitaxial heterostructures of (111)-oriented $LaAlO_3/SrTiO_3$ (LAO/STO). We find that during heterostructure growth, the LAO overlayer eliminates the structural reconstruction of the STO (111) surface with an electronic reconstruction, which determines the properties of the resulting two-dimensional conducting gas. This is confirmed by transport measurements, direct determination of the structure and atomic charge from coherent Bragg rod analysis, and theoretical calculations of electronic and structural characteristics. Interfacial behaviors of the kind discussed here may lead to new growth control parameters useful for electronic devices.

Advances in the fabrication of complex oxide materials, which now can be grown with nearly atomic-scale precision, drive discoveries of novel and exciting phenomena, promising new functionalities, and device concepts. Especially interesting are oxide interfaces with unique electronic, magnetic, and transport properties.[4–9] The atomically smooth interfaces offer a degree of control over decisive interfacial material characteristics, such as lattice constants, carrier concentration, exchange and correlation effects, and spin–orbit coupling not easily attainable in other systems. The crystallographic orientation of this interface plays a surprisingly strategic role, providing unexpected functionalities.[10,11] Interfaces exhibiting hexagonal point group symmetry, such as the (111) in pseudocubic systems, can present entirely new phenomena. For instance, a topologically protected state, which can be tuned by changing dopant ions, substrates, and external gate voltages, has been predicted to exist at (111) perovskite heterostructures.[1–3]

An additional degree of freedom is the polarity of the heterostructure, which must be screened through either atomic or electronic reconstruction to avoid a polar catastrophe. Moving beyond the [001] stacking direction brings new polarity considerations. For example, (111) surfaces of all single-phase insulating perovskite oxides are polar and so creating a (111) interface joins two polar materials—a polar/polar interface. Polar/polar interfaces bring greater flexibility in control over electronic, magnetic, and structural reconstruction phenomena and hence novel properties and functionalities.[12]

The structural and charge transfer configuration in the [111] direction is responsible for these characteristics. When stacked along the [111] direction, an ABO_3 perovskite unit cell consists of three charge transfer bilayers, each containing one oxide AO_3 plane and one metallic B plane, with hexagonally coordinated A and B ions. The bilayers are spaced by $a/\sqrt{3}$, where a is the lattice constant of the (001) unit cell [Fig. 1(a)]. Three offset bilayers form the (111) unit cell. As in (001) interfaces, charges transferred to the interface reside in bands originating from the states on the B-site ions, e.g., Ti in $SrTiO_3$. These determine the charge distribution and electronic properties of the interface as in [001]-oriented heterostructures,[13–17] but there are significant differences. The hexagonal Ti coordination within a (111) plane at the interface and the honeycomb-like structure of two neighboring Ti layers control the electronic structure for two-dimensional carrier sheets confined to the interface. Figure 1(b) shows the projected Ti ionic charge density derived from surface x-ray diffraction and Coherent Bragg Rod Analysis (COBRA) measurements (see the supplementary material for details of COBRA), revealing the honeycomb basis of the Ti electronic structure (see the supplementary material, Fig. S1).

Investigations have revealed characteristics of oxide interfaces unique to the [111] orientation of the LAO/STO interface including those arising in superconductivity,[18,19] in correlation effects,[20,21] and in structural deformations.[22–25] Direct visualization of the interfacial conducting layer[26] by electron holography shows electrons at the interface in both orientations, with an increased spatial extent of the (111) 2DEG compared to (001). Antiferroelastic and polar distortions have been shown to interact differently in the [111] orientation.[27] However, the impact of polarity in the [111] orientation on interface structure and its evolution during heterostructure growth, and on the resulting interfacial 2DEG, still holds surprises. Our experimental and theoretical results indicate that the bilayer interface evolves during growth to become different than the isolated (111) $SrTiO_3$ surface and that this affects the interfacial conducting layer.

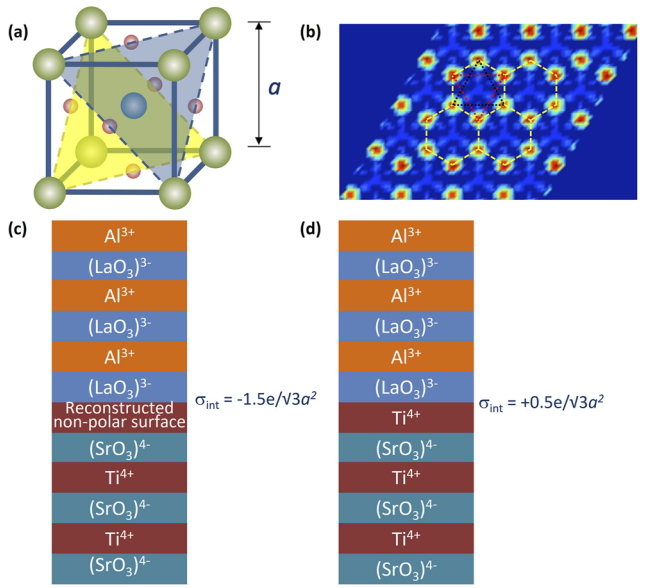

FIG. 1. Stacking sequence along the [111] direction. (a) Schematic diagram of the stacking sequence of LAO and STO along the [111] direction in a ABO_3 cubic perovskite lattice. Yellow, blue, and red planes are the SrO_3 layer of the three offset bilayers. Ti atoms are located between these layers. (b) Ti charge density at the (111) interface obtained by COBRA as viewed along the [111] direction. (c) and (d) Schematic diagram of possible layer structures with charge densities, oscillating internal electric field distribution, and resultant potential build-up involving atomically reconstructed (c) and unreconstructed (d) interfaces.

ABO_3 cubic perovskites are intrinsically polar along the [111] direction in which internal electric fields arise from the alternating AO_3 ($-q$) and B ($+q$) charged layers.[28,29] In these and other materials, surface structural reconstruction can occur.[30] For instance, our COBRA measurements of the layer-resolved charge density of the bare (111) STO substrate (see the supplementary material) indicate a reconstruction of the topmost two sets of those layers that provide the needed depolarizing charge in this single-layer structure. Our measurements of the (111) LAO/STO bilayer heterostructure indicate a different scenario in which the growth of the $LaAlO_3$ overlayer alters the interface, providing instead a global electronic reconstruction across the entire heterostructure. As we now show, the interface structure directly determines the properties of the interfacial conducting gas, perhaps the most immediate being its electron or hole nature.

Figures 1(c) and 1(d) schematically show how two polar perovskites can meet along the [111] direction at a structurally reconstructed [Fig. 1(c)] or non-reconstructed [Fig. 1(d)] interface. In Fig. 1(c), this reconstructed non-polar STO (111) surface acts like the charge neutral STO (001) surface,[12] and the LAO polarity leads to an equivalent interfacial charge density of $-1.5e/\sqrt{3}a^2$. This represents an average electric field pointing toward the LAO/STO interface. In this case, p-type carriers at the interface are required to oppose the electric field within the LAO layer. On the other hand, if the interface is non-reconstructed as in Fig. 1(d), the polar discontinuity at the interface is reduced, with an equivalent charge density of $+0.5e/\sqrt{3}a^2$. Opposite to that in Fig. 1(c), it produces an electric field pointing away from the LAO/STO interface. n-type carriers are required to alleviate the effects of this polarity. Thus, the nature of the interface directly determines the charge density and sign of the interfacial carriers.

We have fabricated epitaxial LAO/STO heterostructures by growing LAO on atomically smooth STO (111) with atomic layer controlled pulsed-laser-deposition as described in the supplementary material. The LAO thickness and crystallinity were monitored by *in situ* reflection high-energy electron diffraction (RHEED) during the growth. The intensity oscillation of the specular spot as a function of time in Fig. 2(a), which has been obtained with the electron propagation parallel to the STO $[1\bar{1}0]$ direction, confirms the layer-by-layer growth of LAO films. Nearly constant amplitude after the first few intensity oscillations reveals that the LAO (111) film surface is smooth. The RHEED pattern in the inset of Fig. 2(b) captured beyond the 20th oscillation indicates epitaxial and coherent growth of LAO. Figure 2(b) shows the atomic force microscopy (AFM) images of an STO substrate chemically and thermally treated to result in Ti-termination[31] and the LAO overlayer. Both STO and LAO surfaces exhibit clear step and terrace structures with the step height of 2.26 and 2.20 Å, respectively, as revealed by line-profiles across the step edges. It is known that LAO films grow unit cell by

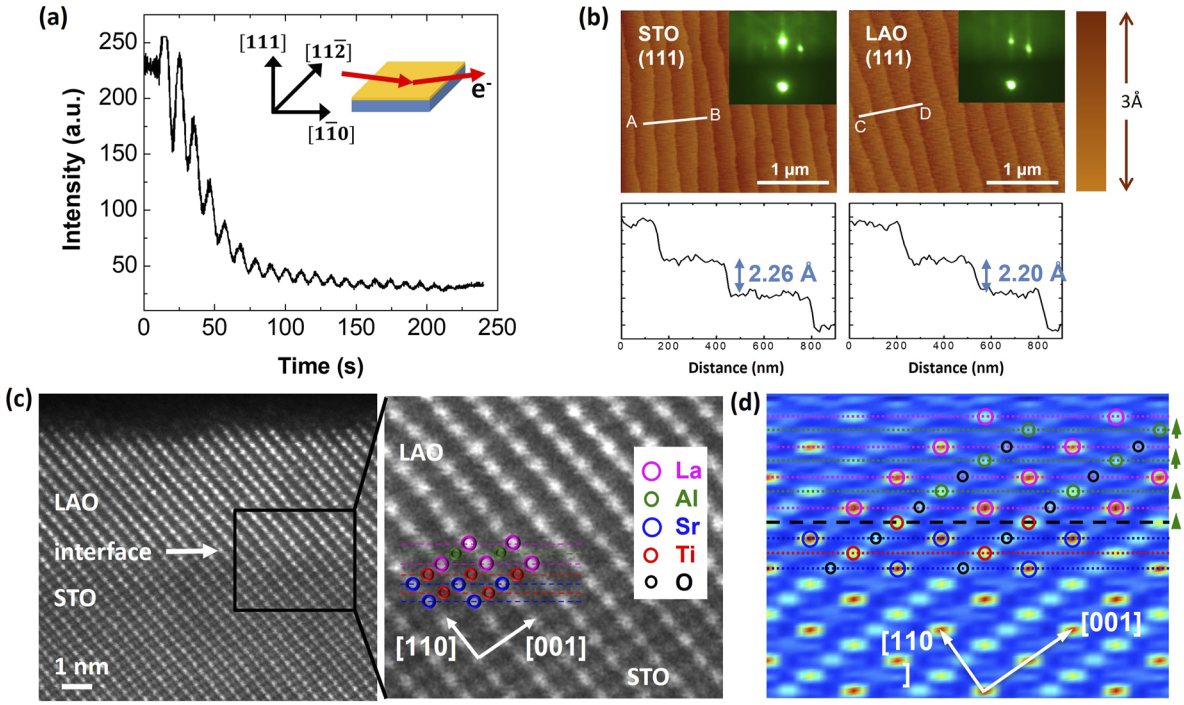

FIG. 2. Atomically smooth epitaxial 20 bilayer LAO film on STO (111) surface. (a) The intensity oscillation of specula RHEED pattern with the electron beam parallel to $[1\bar{1}0]$ direction. It indicates that LAO grows with layer-by-layer growth mode on STO (111) surface. The number of laser pulses, which is required to form one bilayer, is almost half of the one for LAO/STO (001) heterostructure. (b) AFM images of the atomically smooth STO surface after chemical etching and thermal annealing (left) and LAO surface after the growth (right). The inset shows the RHEED image taken along the $[11\bar{2}]$ direction after obtaining 20 intensity oscillations. Surface line profiles along A–B for STO and C–D for LAO are provided. (c) High-resolution dark field STEM image of the coherent interface with [110] zone axis. Green, blue, red, yellow, and black circles are Sr, La, Ti, Al, and O, respectively. The dashed line is the guide for the interface. The average bilayer spacing is 2.15 Å. (d) Charge density map of a plane slice of a three bilayer LAO/STO heterostructure in the same crystallographic direction as (c), constructed by 3D COBRA. Note that the location of oxygen atoms is distinguishable by the electron density distribution from COBRA contrary to the projected STEM image. STEM images are background filtered.

unit cell on STO (001) and one RHEED intensity oscillation corresponds to one unit cell (uc) of LAO (3.792 Å) along the [001] direction.[32] However, as revealed by the step height in AFM, this is likely not the case for [111] growth. Figure 2(c) shows the high-resolution dark field STEM image of an epitaxial LAO film grown on STO (111) surface with 20 RHEED intensity oscillations. The bright spots are heavy La atoms, which form 20 rows above the STO substrate, indicating that one RHEED intensity oscillation corresponds to one bilayer of $(LaO_3)^{3-}$ and Al^{3+} with the thickness of 2.19 Å. We consider the LaO_3–Al bilayer as a basic unit and discuss our results in terms of the number of these bilayers. Note that in the same sense, the LaO–AlO_2 bilayer can also be regarded as a basic unit for [001] orientation. In this [001] orientation, the unit cell consists of a single LaO–AlO_2 bilayer, so the number of unit cells matches the number of bilayers.

Both [111]- and [001]-oriented heterostructures were evaluated with variable temperature magnetotransport measurements. Hall measurements, using wire-bonded van der Pauw configurations and also patterned Hall bar configurations, gave consistent results, showing *n*-type mobile carriers above the LAO critical thickness. The critical thickness and other transport properties were determined by temperature-dependent transport measurements with varying LAO overlayer thicknesses. The (111) heterostructure with 20 LAO bilayers has a conducting interface with a sheet resistance comparable to LAO/STO (001) heterostructures. For comparison, we also measured the transport of LAO/STO (001) interface and evaluated in terms of the number of bilayers along the [001] direction.

The (111) interface is insulating below six bilayers and completely conducting above 15 bilayers [see Figs. S3(a) and S3(b)]. The two-dimensional sheet carrier concentration [n_s, Fig. S3(b)] in the conducting region is higher than that of similarly prepared LAO/STO (001); however, both R_s and n_s have a transition between the insulating and conducting state broader compared to LAO/STO (001) [see Fig. S3(b)] that has a sharp transition near four bilayers of the LAO overlayer.[33] The room temperature mobility is comparable but smaller than that of LAO/STO (001) interface. Brinks *et al.* have shown that the LAO/STO (001) interfacial 2DEG shows in-plane transport anisotropy.[34] However, our measurements of Hall bar patterned samples show no anisotropy of the LAO/STO (111) 2DEG between in-plane (100) and (010). Previous temperature-dependent measurements found anisotropy in (111) heterostructures only at

low temperature.[35] Variable temperature transport characteristics [Figs. S3(c) and S3(d)] show that the mobility of LAO/STO (001) at low temperatures is higher than that of LAO/STO (111), with similar interfacial carrier concentrations.

These magnetotransport measurements indicate that the LAO/STO (111) heterointerface has a non-reconstructed polar interface as suggested in Fig. 1(d). This modified interface charge density and the electric field as discussed earlier also affect the LAO critical thickness. Due to the reduced internal field represented by the equivalent interface and surface charge densities, the critical thickness in the electronic reconstruction scenario[36] is increased by a factor of $\sqrt{3}$ as compared to LAO/STO (001). The bilayer spacing is $\sqrt{3}$ times smaller in the [111] orientation as compared to the bilayer spacing in the [001] so that the critical thickness in a number of bilayers is expected to be three times greater in the [111] orientation. A critical thickness of 3 uc (3 [001] bilayers) for LAO/STO (001) results in the prediction of nine bilayers of the critical thickness along the [111] direction.

This interpretation is verified by density functional theory (DFT) calculations (see the supplementary material for details). The layer-resolved density of states calculation in Fig. 3 shows the transition from insulating to conducting. The LAO/STO heterointerface is insulating when six bilayers are deposited, while it becomes metallic as the thickness increases up to eight bilayers. This is evident from the Fermi energy lying in the bandgap for the six bilayer heterostructure [Fig. 3(a)] and in the Ti 3d conduction band for the eight bilayer heterostructure [Fig. 3(b)]. The dashed line showing the AO_3 valence band edge is indicative of the average internal electric field of the LAO layer and of zero electric field in the STO layers.

As described previously, *n*-type carriers at the (111) LAO/STO interface would arise in response to an LAO internal electric field pointing away from the interface.[37,38] Our direct structural evidence confirms this direction of the internal E-field. Three-dimensional atomic positions above and below the (111) LAO/STO interface were determined by synchrotron x-ray diffraction at the Advanced Photon Source. *L*-scans along seven symmetry non-equivalent crystal truncation rods (CTRs) were performed for both an insulating interface with three bilayers and a conducting interface with 20 bilayers (see the supplementary material). The total film thickness and the average bilayer thickness of the 20 bilayer LAO film are calculated from the thickness fringes to be 43.8 and 2.19 Å, respectively, consistent with values determined from the TEM analysis. COBRA allows us to determine atomic positions from the three-dimensional charge density and to estimate layer occupancy and stoichiometry from layer-integrated electron densities.

Figure 2(d) shows a slice through the three-dimensional charge density perpendicular to the LAO/STO interface of the three bilayer LAO film. The positively charged Al layer in the LAO is not centered between the negatively charged LaO_3 layers but has an offset in the direction away from the interface. This offset can be understood as an atomic rumpling to depolarize the electric field, which is induced by the polar nature of the LAO film. For LAO/STO (100) heterostructures, buckling in AO and BO_2 planes plays this role.[38–41] This is quantified in Fig. 4(a), where a positive B-site off-center displacement corresponds to displacement away from the center of the adjacent two A-site cations. The 20 bilayer conducting film shows small, mixed B-site off center displacements above the interface [Fig. 4(b)], implying a suppressed electric field inside the LAO layers. This is because the heterostructure no longer requires depolarization by rumpling once the LAO thickness exceeds the critical value for 2DEG formation. DFT calculations as discussed above were also completed for 3 and 20 bilayer LAO heterostructures. The calculated

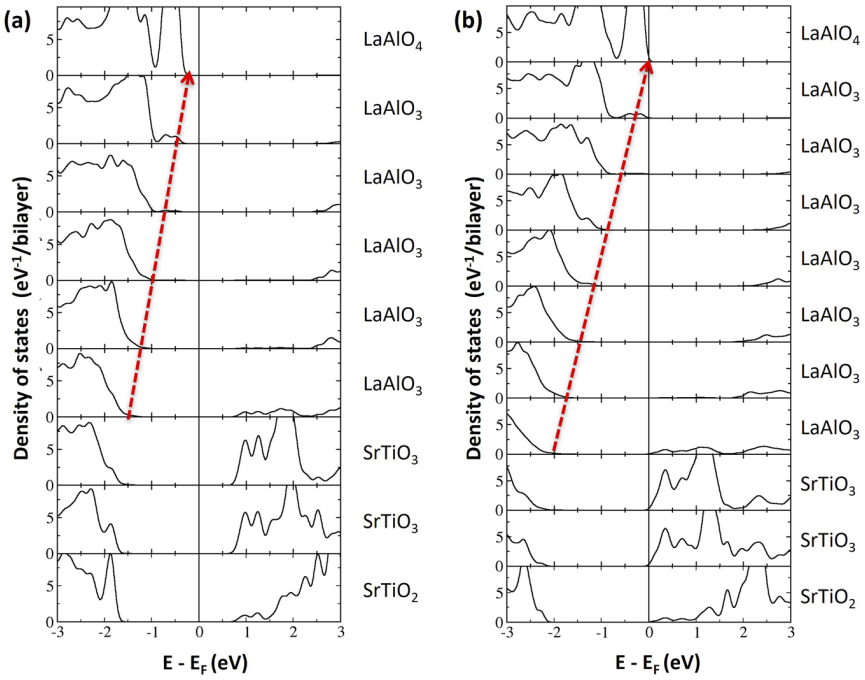

FIG. 3. DFT calculations. Bilayer-resolved density of states for six bilayer (a) and eight bilayer (b) LAO films. The solid black line at zero in the x axis indicates the Fermi energy. The red dashed arrows indicate the electrostatic potential in LAO films. The eight bilayer LAO produces electronic reconstruction by transferring an electron charge from the LAO surface to STO, as is evident from the Fermi energy lying above the conduction band minimum of STO.

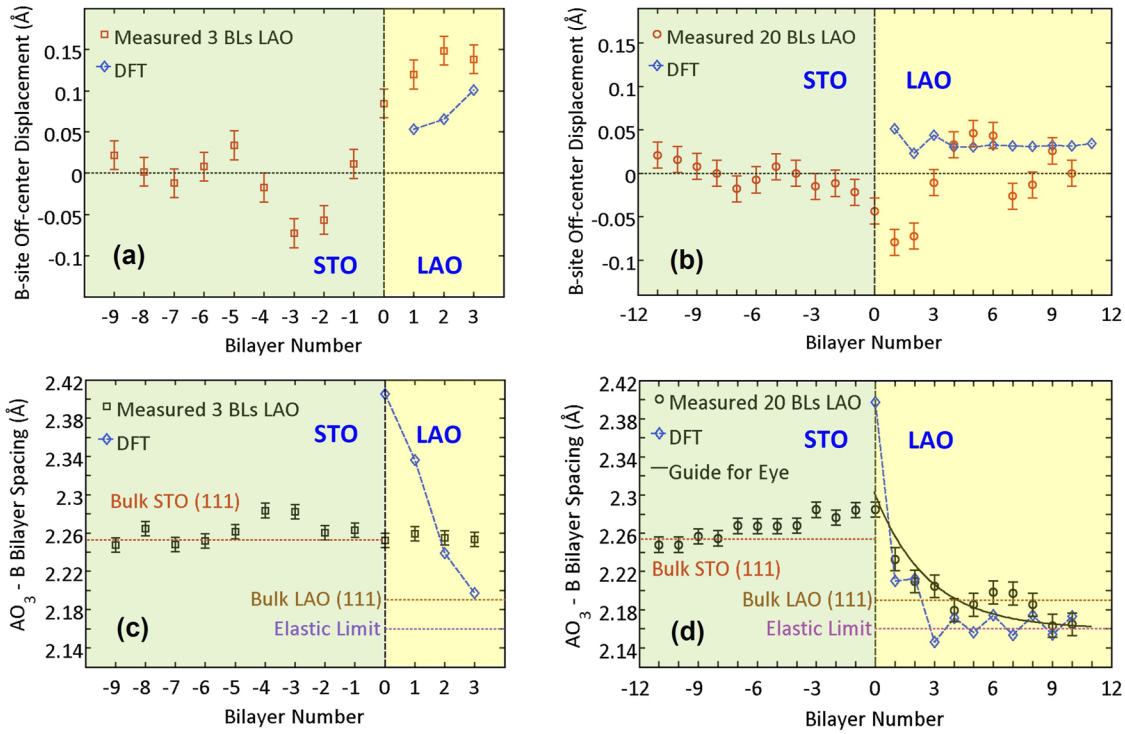

FIG. 4. Determination of the detailed layer structure by COBRA. B-site off-center relative displacement of the insulating three bilayer LAO (a) and the conducting 20 bilayer LAO films (b). Bilayer spacing of the insulating three bilayer LAO (c) and the conducting 20 bilayer LAO films (d). Values from the DFT calculations are overlaid.

B-site off-center displacements are shown in the figure, consistent with the experimental results.

As shown in Figs. 4(c) and 4(d), the bilayer lattice spacing of the insulating three bilayer LAO film is not in the elastic limit and is significantly larger than the value predicted based on pure elasticity of the LAO film even though it is under tensile strain. In contrast, the conducting 20 bilayer LAO film shows a gradual decrease of the LAO bilayer lattice spacing approaching the elastic limit determined by the Poisson ratio of LAO, 0.24.[42] The average value is close to 2.19 Å. The significant difference of the lattice spacing of the two LAO films also points to a large change of electric field inside the LAO layer as it undergoes a transition from insulating to conducting state, and the electrostriction by the different polarity between LAO and STO should induce the large lattice spacing at thin LAO films.[31,43] The DFT calculation supports this result as indicated by the calculated bilayer spacings shown.

Our experimental COBRA evidence [Figs. 5(c) and 5(d)] indicates that LAO/STO (111) preserves AO_3/B layer stacking without atomic reconstruction at the interface, while a bare STO (111) surface exhibits surface reconstruction and off-stoichiometry [Figs. 5(a) and 5(b)] as in TEM analysis.[44] The bare STO (111) surface shows non-trivial CTR intensity variations [significant bumps in Fig. S2(a)] between Bragg peaks, which should not appear without surface reconstruction. Figure 5(a) shows the electron density profile of this bare STO (111) surface determined from the CTR and the COBRA method, with electron density variation near the surface layers indicative of surface modifications. The significant change in stoichiometry of subsurface SrO_3 and Ti layers and small lattice distortions effectively compensates the diverging surface electrostatic energy [Fig. 5(b)]. The 80% layer occupancy of the first Ti layer could indicate a 3 × 3 surface reconstruction observed by both TEM and STM studies.[30] Figures 5(c) and 5(d) indicate that the LAO/STO (111) heterostructures have no structural reconstruction at the LAO/STO interface. One possible explanation is that the high energy particles in the laser-ablation plume diffuse into the substrate and elevate the original reconstructed surface structure, allowing an unreconstructed interface to form. Interfacial intermixing or oxygen point defects would not affect this interfacial process, although the somewhat higher saturated carrier concentration of LAO/STO (111) as compared to LAO/STO (100) in Fig. S3(b) is indicative of a surface with higher propensity toward atomic defects that could supply electrons to the interface. This type of floating surface reconstruction has been investigated by STM studies of homoepitaxial STO layers on Nb-doped STO substrates.[45] *In situ* surface x-ray scattering combined with the LAO film growth could elucidate this phenomenon in the (111) orientation, as recently reported for (001).[46]

We have reported a global electronic reconstruction in LAO/STO (111) heterostructures not found in other crystallographic orientations, supported by detailed x-ray structural determination, electrical transport characterization, and theoretical calculations. This work can be expanded to the study of artificial stacking

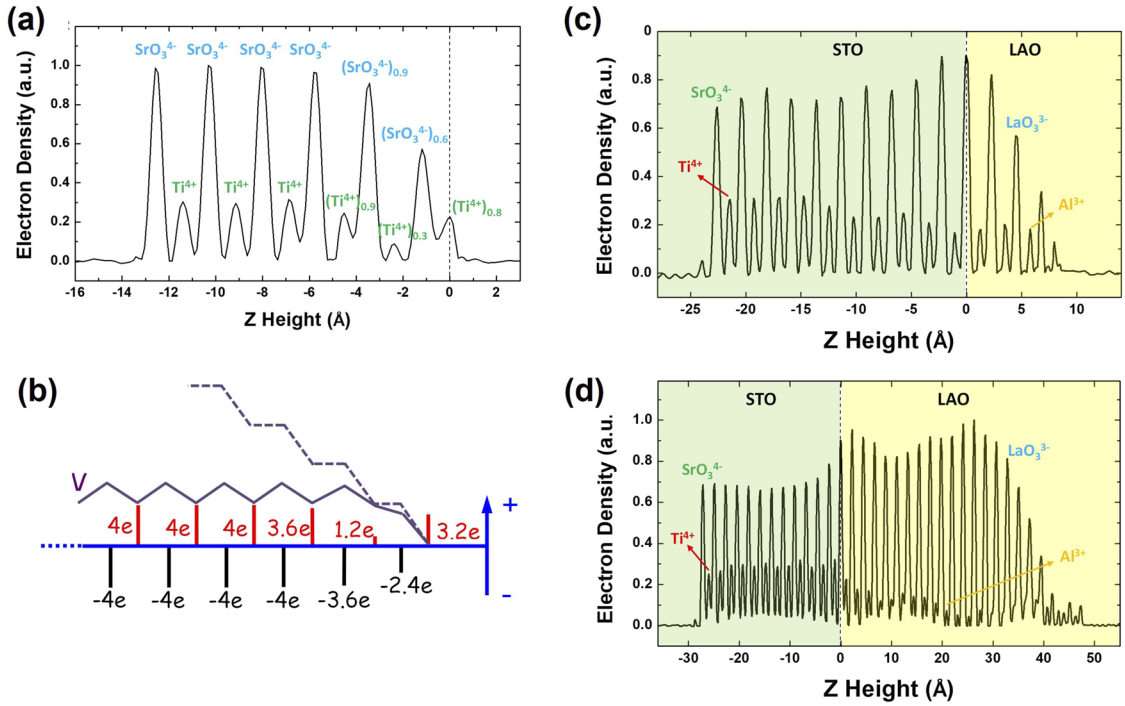

FIG. 5. (a) Experimentally determined electron density profile of the treated bare $SrTiO_3$ (111) surface. (b) The diagram of the charge distribution and electrostatic potential near the surface of $SrTiO_3$ (111). Possible surface reconstruction (top Ti layer) and subsurface off-stoichiometry (SrO_3 and Ti layer deficiency) alleviate a polar catastrophe in the bare substrate, as illustrated by the dashed line, of the intrinsically polar (111) system. Electron density profiles of the three bilayers (c) and 20 bilayers of LAO (d) as a function of *z* height, showing an interface with no structural reconstruction. Intensity drops near the top surface of LAO films suggest incomplete coverage.

of general polar surfaces including non-oxide materials, such as graphene on (111) cubic lattice planes and topologically protected edge states[47,48] at the interface of oxide materials with enhanced spin–orbit coupling. These are expected to stimulate new directions and features in condensed-matter physics and to provide new opportunities in manipulation of layered perovskites. In addition, the understanding of the important building block of the (111) heterointerface will allow for the design and development of new interfacial multifunctionalities.

See the supplementary material for methods of heterostructure fabrication, transport measurements, theoretical modeling, and COBRA analysis of x-ray surface diffraction.

This research was funded by the Gordon and Betty Moore Foundation's EPiQS Initiative (Grant No. GBMF9065) to C.B.E., the Vannevar Bush Faculty Fellowship (Grant No. N00014-20-1-2844), AFOSR (Grant No. FA9550-15-1-0334), and NSF through the University of Wisconsin MRSEC [Grant No. DMR-1720415 (C.B.E.)]. Transport measurements at the University of Wisconsin–Madison were supported by the U.S. Department of Energy (DOE), Office of Science, Office of Basic Energy Sciences (BES), under Award No. DE-FG02-06ER46327. The research at the University of Nebraska-Lincoln (UNL) was supported by the NSF through MRSEC (Grant No. DMR-0820521) and EPSCoR RII Track-1 (Grant No. OIA-2044049) programs. Computations were performed at the UNL's Holland Computing Center and Center for Nanophase Materials Sciences at Oak Ridge National Laboratory. D.D.F. was supported by the U.S. Department of Energy Office of Basic Energy Sciences (BES), Materials Science and Engineering Division. The use of the Advanced Photon Source at Argonne National Laboratory was supported by the U.S. Department of Energy (DOE), Basic Energy Sciences, under Contract No. DE-AC02-06CH11357.

AUTHOR DECLARATIONS

Conflict of Interest

The authors have no conflicts to disclose.

Author Contributions

S.R., C.W.B., and J.P. fabricated the samples and analyzed the structure and surfaces by x-ray diffraction and AFM. N.C. and T.H. carried out electrical transport characterizations. T.R.P. performed theoretical calculations of electronic and structural characteristics under supervision of E.Y.T. H.Z. and D.D.F. carried out synchrotron characterizations and determined the structure and charge distributions by COBRA. Y.Z. and L.X. carried out TEM measurements. S.R. prepared the manuscript. C.B.E., M.S.R., H.Z., D.D.F., and X.Q.P. supervised the experiments and with E.Y.T. contributed to manuscript preparation. C.B.E. conceived and directed the research. All authors discussed the results and implications and commented on the manuscript at all stages.

DATA AVAILABILITY

The data that support the findings of this study are available within the article and its supplementary material, and additional data are available from the corresponding author upon reasonable request.

REFERENCES

[1] D. Xiao, W. Zhu, Y. Ran, N. Nagaosa, and S. Okamoto, Nat. Commun. **2**, 596 (2011).
[2] A. Rüegg and G. A. Fiete, Phys. Rev. B **84**, 201103(R) (2011).
[3] J. Chakhalian, A. J. Millis, and J. Rondinelli, Nat. Mater. **11**, 92 (2012).
[4] J. Mannhart and D. G. Schlom, Science **327**, 1607 (2010).
[5] P. Zubko, S. Gariglio, M. Gabay, P. Ghosez, and J.-M. Triscone, Annu. Rev. Condens. Matter Phys. **2**, 141 (2011).
[6] H. Y. Hwang, Y. Iwasa, M. Kawasaki, B. Keimer, N. Nagaosa, and Y. Tokura, Nat. Mater. **11**, 103 (2012).
[7] J. Pereiro, A. T. Bollinger, G. Logvenov, A. Gozar, C. Panagopoulos, and I. Božović, Philos. Trans. R. Soc. London, Ser. A **370**, 4890 (2012).
[8] S. Gariglio, M. Gabay, and J.-M. Triscone, APL Mater. **4**, 060701 (2016).
[9] H. Lee, N. Campbell, J. Lee, T. J. Asel, T. R. Paudel, H. Zhou, J. W. Lee, B. Noesges, J. Seo, B. Park, L. J. Brillson, S. H. Oh, E. Y. Tsymbal, M. S. Rzchowski, and C. B. Eom, Nat. Mater. **17**, 231 (2018).
[10] A. Grutter, F. Wong, E. Arenholz, M. Liberati, A. Vailionis, and Y. Suzuki, Appl. Phys. Lett. **96**, 082509 (2010).
[11] M. Gibert, P. Zubko, R. Scherwitzl, J. Íñiguez, and J.-M. Triscone, Nat. Mater. **11**, 195 (2012).
[12] C. W. Bark, D. A. Felker, Y. Wang, Y. Zhang, H. W. Jang, C. M. Folkman, J. W. Park, S. H. Baek, H. Zhou, D. D. Fong, X. Q. Pan, E. Y. Tsymbal, M. S. Rzchowski, and C. B. Eom, Proc. Natl. Acad. Sci. U. S. A. **108**, 4720 (2011).
[13] A. Ohtomo and H. Y. Hwang, Nature **427**, 423 (2004).
[14] N. Nakagawa, H. Y. Hwang, and D. A. Muller, Nat. Mater. **5**, 204 (2006).
[15] A. Brinkman, M. Huijben, M. van Zalk, J. Huijben, U. Zeitler, J. C. Maan, W. G. van der Wiel, G. Rijnders, D. H. A. Blank, and H. Hilgenkamp, Nat. Mater. **6**, 493 (2007).
[16] N. Reyren, S. Thiel, A. D. Caviglia, L. Fitting Kourkoutis, G. Hammerl, C. Richter, C. W. Schneider, T. Kopp, A.-S. Rüetschi, D. Jaccard, M. Gabay, D. A. Muller, J.-M. Triscone, and J. Mannhart, Science **317**, 1196 (2007).
[17] P. Irvin, Y. Ma, D. F. Bogorin, C. Cen, C. W. Bark, C. M. Folkman, C.-B. Eom, and J. Levy, Nat. Photonics **4**, 849 (2010).
[18] A. M. R. V. L. Monteiro, D. J. Groenendijk, I. Groen, J. de Bruijckere, R. Gaudenzi, H. S. J. van der Zant, and A. D. Caviglia, Phys. Rev. B **96**, 020504(R) (2017).
[19] P. K. Rout, E. Maniv, and Y. Dagan, Phys. Rev. Lett. **119**, 237002 (2017).
[20] U. Khanna, P. K. Rout, M. Mograbi, G. Tuvia, I. Leermakers, U. Zeitler, Y. Dagan, and M. Goldstein, Phys. Rev. Lett. **123**, 036805 (2019).
[21] M. R. V. L. Monteiro, M. Vivek, D. J. Groenendijk, P. Bruneel, I. Leermakers, U. Zeitler, M. Gabay, and A. D. Caviglia, Phys. Rev. B **99**, 201102(R) (2019).
[22] D. Doennig, W. E. Pickett, and R. Pentcheva, Phys. Rev. Lett. **111**, 126804 (2013).
[23] C. Li, Q. Xu, Z. Wen, S. Zhang, A. Li, and D. Wu, Appl. Phys. Lett. **103**, 201602 (2013).
[24] C. Bareille, F. Fortuna, T. C. Rödel, F. Bertran, M. Gabay, O. Hijano Cubelos, A. Taleb-Ibrahimi, P. Le Fèvre, M. Bibes, A. Barthélémy, T. Maroutian, P. Lecoeur, M. J. Rozenberg, and A. F. Santander-Syro, Sci. Rep. **4**, 3586 (2014).
[25] G. Herranz, F. Sánchez, N. Dix, M. Scigaj, and J. Fontcuberta, Sci. Rep. **2**, 758 (2012).
[26] K. Song, S. Ryu, H. Lee, T. R. Paudel, C. T. Koch, B. Park, J. K. Lee, S.-Y. Choi, Y.-M. Kim, J. C. Kim, H. Y. Jeong, M. S. Rzchowski, E. Y. Tsymbal, C.-B. Eom, and S. H. Oh, Nat. Nanotechnol. **13**, 198 (2018).
[27] T. Min, W. Choi, J. Seo, G. Han, K. Song, S. Ryu, H. Lee, J. Lee, K. Eom, C. B. Eom, H. Y. Jeong, Y.-M. Kim, J. Lee, and S. H. Oh, Sci. Adv. **7**, eabe9053 (2021).
[28] M. Kawasaki, K. Takahashi, T. Maeda, R. Tsuchiya, M. Shinohara, O. Ishiyama, T. Yonezawa, M. Yoshimoto, and H. Koinuma, Science **266**, 1540 (1994).
[29] I. V. Maznichenko, S. Ostanin, A. Ernst, J. Henk, and I. Mertig, Phys. Status Solidi B **257**, 1900540 (2020).
[30] X. Torrelles, G. Cantele, G. M. De Luca, R. Di Capua, J. Drnec, R. Felici, D. Ninno, G. Herranz, and M. Salluzzo, Phys. Rev. B **99**, 205421 (2019).
[31] A. Biswas, P. B. Rossen, C.-H. Yang, W. Siemons, M.-H. Jung, I. K. Yang, R. Ramesh, and Y. H. Jeong, Appl. Phys. Lett. **98**, 051904 (2011).
[32] M. Huijben, A. Brinkman, G. Koster, G. Rijnders, H. Hilgenkamp, and D. H. A. Blank, Adv. Mater. **21**, 1665 (2009).
[33] S. Thiel, G. Hammerl, A. Schmehl, C. W. Schneider, and J. Mannhart, Science **313**, 1942 (2006).
[34] P. Brinks, W. Siemons, J. E. Kleibeuker, G. Koster, G. Rijnders, and M. Huijben, Appl. Phys. Lett. **98**, 242904 (2011).
[35] S. Davis, V. Chandrasekhar, Z. Huang, K. Han, and T. Venkatesan, Phys. Rev. B **95**, 035127 (2017).
[36] H. Chen, A. M. Kolpak, and S. Ismail-Beigi, Adv. Mater. **22**, 2881 (2010).
[37] R. Pentcheva and W. E. Pickett, Phys. Rev. Lett. **102**, 107602 (2009).
[38] S. A. Pauli, S. J. Leake, B. Delley, M. Björck, C. W. Schneider, C. M. Schlepütz, D. Martoccia, S. Paetel, J. Mannhart, and P. R. Willmott, Phys. Rev. Lett. **106**, 036101 (2011).
[39] R. Yamamoto, C. Bell, Y. Hikita, H. Y. Hwang, H. Nakamura, T. Kimura, and Y. Wakabayashi, Phys. Rev. Lett. **107**, 036104 (2011).
[40] C. Cantoni, J. Gazquez, F. Miletto Granozio, M. P. Oxley, M. Varela, A. R. Lupini, S. J. Pennycook, C. Aruta, U. S. di Uccio, P. Perna, and D. Maccariello, Adv. Mater. **24**, 3952 (2012).
[41] C. Cancellieri, D. Fontaine, S. Gariglio, N. Reyren, A. D. Caviglia, A. Fête, S. J. Leake, S. A. Pauli, P. R. Willmott, M. Stengel, Ph. Ghosez, and J.-M. Triscone, Phys. Rev. Lett. **107**, 056102 (2011).
[42] X. Luo and B. Wang, J. Appl. Phys. **104**, 073518 (2008).
[43] Z. S. Popović, S. Satpathy, and R. M. Martin, Phys. Rev. Lett. **101**, 256801 (2008).
[44] A. N. Chiaramonti, B. C. Russell, M. R. Castell, A. K. Subramanian, K. R. Poeppelmeier, P. C. Stair, and L. D. Marks, Microsc. Microanal. **12**, 1230 (2006).
[45] R. Shimizu, K. Iwaya, T. Ohsawa, S. Shiraki, T. Hasegawa, T. Hashizume, and T. Hitosugi, ACS Nano **5**, 7967 (2011).
[46] S. Cook, K. Letchworth-Weaver, I.-C. Tung, T. K. Andersen, H. Hong, L. D. Marks, and D. D. Fong, Sci. Adv. **5**, eaav0764 (2019).
[47] L. Fu, C. L. Kane, and E. J. Mele, Phys. Rev. Lett. **98**, 106803 (2007).
[48] H. Zhang, C.-X. Liu, X.-L. Qi, X. Dai, Z. Fang, and S.-C. Zhang, Nat. Phys. **5**, 438 (2009).